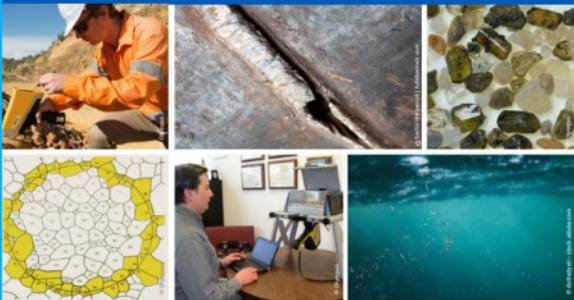




2nd Advanced Optical Metrology Compendium

Advanced Optical Metrology

Geoscience | Corrosion | Particles | Additive Manufacturing: Metallurgy, Cut Analysis & Porosity



EVIDENT
OLYMPUS

WILEY

The latest eBook from **Advanced Optical Metrology**.
Download for free.

This compendium includes a collection of optical metrology papers, a repository of teaching materials, and instructions on how to publish scientific achievements.

With the aim of improving communication between fundamental research and industrial applications in the field of optical metrology we have collected and organized existing information and made it more accessible and useful for researchers and practitioners.

EVIDENT
OLYMPUS

WILEY

An Atomistic View of Platinum Cluster Growth on Pristine and Defective Graphene Supports

Julia Bord, Björn Kirchhoff, Matthias Baldofski, Christoph Jung,* and Timo Jacob*


Density functional theory (DFT) is used to systematically investigate the electronic structure of platinum clusters grown on different graphene substrates. Platinum clusters with 1 to 10 atoms and graphene vacancy defect supports with 0 to 5 missing C atoms are investigated. Calculations show that Pt clusters bind more strongly as the vacancy size increases. For a given defect size, increasing the cluster size leads to more endothermic energy of formation, suggesting a templating effect that limits cluster growth. The opposite trend is observed for defect-free graphene where the formation energy becomes more exothermic with increasing cluster size. Calculations show that oxidation of the defect weakens binding of the Pt cluster, hence it is suggested that oxygen-free graphene supports are critical for successful attachment of Pt to carbon-based substrates. However, once the combined material is formed, oxygen adsorption is more favorable on the cluster than on the support, indicating resistance to oxidative support degradation. Finally, while highly-symmetric defects are found to encourage formation of symmetric Pt clusters, calculations also reveal that cluster stability in this size range mostly depends on the number of and ratio between Pt–C, Pt–Pt, and Pt–O bonds; the actual cluster geometry seems secondary.

J. Bord, B. Kirchhoff, C. Jung, T. Jacob
Institute of Electrochemistry
Ulm University
Albert-Einstein-Allee 47 89081, Ulm, Germany
E-mail: christoph.jung@kit.edu; timo.jacob@uni-ulm.de

M. Baldofski
Freudenberg Technology Innovation SE & Co. KG
Hoehnerweg 2-4 69469, Weinheim, Germany
M. Baldofski
Fraunhofer-Institute for Mechanics of Materials IWM
Wöhlerstraße 11 79108, Freiburg, Germany

C. Jung, T. Jacob
Helmholtz Institute Ulm (HIU) Electrochemical Energy Storage
Helmholtz-Strasse 11 89081, Ulm, Germany

C. Jung, T. Jacob
Karlsruhe Institute of Technology (KIT)
P.O. Box 3640 76021, Karlsruhe, Germany

 The ORCID identification number(s) for the author(s) of this article can be found under <https://doi.org/10.1002/sml.202207484>.

© 2023 The Authors. Small published by Wiley-VCH GmbH. This is an open access article under the terms of the Creative Commons Attribution-NonCommercial-NoDerivs License, which permits use and distribution in any medium, provided the original work is properly cited, the use is non-commercial and no modifications or adaptations are made.

DOI: 10.1002/sml.202207484

1. Introduction

The proton-exchange membrane fuel cell (PEMFC) is an important cornerstone in a new mix of technologies for renewable energy production. To date, nanoparticles (NPs) of transition metals (TMs), still most notably of platinum, are the most active material class for the electro-catalytic oxygen reduction reaction (ORR).^[1–3] In PEMFCs, the rate of the cathodic ORR is significantly slower than that of the anodic hydrogen oxidation reaction (HOR), hence research efforts focus predominantly on the cathode side. Therein, the key challenge is to maximize the mass activity of the electro-catalyst, which means minimizing the mass loading of expensive and non-earth-abundant transition metals while maximizing their catalytic activity.

To this end, state-of-the-art ORR catalysts are employed: i) in nanoparticulate form to maximize the catalyst's surface-to-volume ratio and ii) dispersed on a conductive support. Graphene,^[4,5] carbon

nanotubes,^[6] and carbon black^[7] are preferred catalyst support materials due to their high electrical conductivity, large surface area, and resistance to chemical decomposition.^[8–10] In general, the measured mass activity increases as the supported NPs become smaller. However, NPs of 2 nm size and smaller are unstable on the support surface and therefore they degrade and lose activity rapidly, rendering them unreliable for practical applications.^[11] Degradation mechanisms include ripening processes and agglomeration due to migration and coalescence of small particles.^[11–13] In addition, dissolution processes during catalytic reactions and due to interactions with the electrolyte can lead to material loss.^[11,14–17]

Recent studies have shown that while TM NPs bind weakly to pristine graphene, defect sites in graphene can serve as anchor points that greatly increase binding strength. Interestingly, this anchoring effect is prominent in particular for small TM clusters, which can fit into defects that are only several atoms wide where they covalently bind to the unsaturated carbon atoms.^[4,18] Moreover, several groups were able to show that the support material will not only coordinatively stabilize the clusters, but also modify the reactivity of the resulting combined material.^[4,19–22] This effect was investigated for example for Ni,^[23,24] Fe,^[24,25] Co,^[24] and Au^[26] clusters adsorbed on graphene supports with vacancies.

While clever use of defect anchoring could lead to a significant reduction of the minimum particle size achievable with supported metal catalysts, recent years have seen this concept taken to its logical conclusion: highly-dispersed single atom catalysts (SACs). Within the last 10 years, SACs have developed from a theoretical concept of an idealized system to a highly-active research field thanks to advances in synthetic methods and because they open access to a wide range of unprecedented reactivity.^[27] In terms of important SAC parameters, besides the obvious importance of the embedded element, the influence of the support, too, has come under intense scrutiny; we refer here to a review by Zhuo et al. which summarizes recent computational research on graphene-based supports for SACs in particular.^[28]

Of particular interest for the present work are studies which systematically investigated the interactions of clusters of increasing size with supports with increasing vacancy defect size. A plethora of research is available on SACs or double-atom catalysts (DACs) embedded in vacancies consisting of 1 or 2 missing atoms. Interactions with larger clusters have been studied as well, in particular for “magic number” clusters such as Pt₁₃.^[29] However, only a few studies explored the intermediary cluster size range. One example of such a study is presented by Gao et al. who computationally investigated the growth of nickel NPs consisting of up to ten Ni atoms on graphene supports.^[23] The group considered both defect-free and defective graphenes formed by the removal of up to five adjacent C atoms. Notably, the group highlights in particular that the electronic properties of the Ni cluster change significantly with the size and electronic structure of the vacancy defect of the graphene support. Further, the strong anchoring effect could be rationalized by a Ni-carbide formation within the graphene-plane, followed by symmetric cluster growth on both sides of the support plane.

The significant difference between pristine and vacancy-defective graphene with regards to interaction strength with TM adspecies has been reported on several occasions. For example, Ramos-Sanchez and Balbuena^[30] as well as Yang et al.^[31] found only little evidence of charge transfer from Pt clusters to defect-free graphite and graphene supports. Wang et al. demonstrated that charge transfer from Pt clusters to defect-free carbon nanotubes (CNTs) is also limited but significantly increases when defective CNTs are considered.^[32] The electronic effects of the carbon support—and particularly of the vacancy size—on TM clusters therefore cannot be overstated and warrants detailed investigation. This realization partially motivates the present work.

To complete the motivation for this study, we note that computational research into the stability of SACs and small metal clusters on defective carbon supports against oxidation is, to the best of our knowledge, currently under-represented in literature. Oxidative degradation is of particular importance when such materials are used as ORR electro-catalysts. Furthermore, a popular way to synthesize graphene is via Hummer’s method^[33] where graphite is fully oxidized to graphene oxide to exfoliate individual sheets before subsequent reduction to graphene. The question then becomes how already-oxidized defects, which potentially remain in the final material from synthesis, will influence the stability of deposited TM clusters.

At first glance, it is evident that fuel cell performance will be negatively affected by carbon oxidation as Pt particles may detach as a result, which decreases the active surface area of the catalyst.^[11,13] The interactions between oxidized graphene and Pt clusters, however, can be favorable under certain conditions. Paradoxically, Wu and Ho show that specific ratios of oxygen to carbon can even lead to an enhancement of the adsorption of Pt₁₃ clusters compared to pristine graphene.^[29] The electronic effects on the combined material due to the presence of oxygen, too, are non-trivial. For example, Ma et al. investigated the interactions between small Pt clusters and graphene supports with high or low degree of oxidation.^[34] The group specifically investigated the effects of oxygen-based functional groups on the charge transfer to the Pt cluster, which they found to be maximized in cases where the cluster was in contact with both C atoms and O functional groups at the same time. We are therefore convinced that any study into the activity of TM/graphene combined materials as ORR catalysts also needs to consider the effects of support oxidation.

The focus of the present work is to use DFT calculations to systematically investigate the stability and electronic properties of Pt clusters of increasing size ($n_{\text{Pt}} = 1 - 10$) brought into contact with defective graphene supports which contain vacancies of increasing size ($x_{\text{defect}} = 1 - 5$ C atoms). This investigation is performed in oxygen-free conditions as well as for systems where either the vacancy or the Pt cluster is oxidized. Finally, the calculated trends are discussed with regards to experimental conditions during synthesis and operando stability of the combined material.

2. Results and Discussion

2.1. Interaction of Pt Clusters with Non-Oxidized Graphene Supports

Due to the strong influence of the presence of vacancies in carbon support materials on adsorbed metal NPs and thus on the catalytic properties of the system, it is assumed that the support also plays a key role in the growth of platinum clusters. To investigate the impact of graphene sheets d_x with $x \leq 5$ vacancy defects serving as substrate models (see Figure S1, Supporting Information) on the interaction with Pt particles, DFT calculations are performed. We successively construct Pt_{*n*} clusters with up to $n = 10$ Pt atoms on each of the graphene supports with and without vacancies to model the adsorbed Pt NPs.

The binding energy values are calculated using Equation (1) based on the optimized adsorption configurations with the lowest total energy. The results are summarized in **Figure 1**. Increasing the size of Pt clusters adsorbed on graphene models with C vacancy defects leads to a decrease in binding energy per atom. The binding energy asymptotically approaches the Pt bulk cohesive energy, which we calculated to be 5.49 eV atom⁻¹ (exp: 5.85 eV atom⁻¹).^[35] as the ratio of bulk to surface atoms increases with increasing cluster size.

In addition to the Pt–Pt bonds, the Pt atoms that form σ -bonds with C-sp² orbitals contribute to the total binding energy. This Pt–C σ -interaction results from the presence of vacancies in graphene leading to dangling C–C σ -bonds.

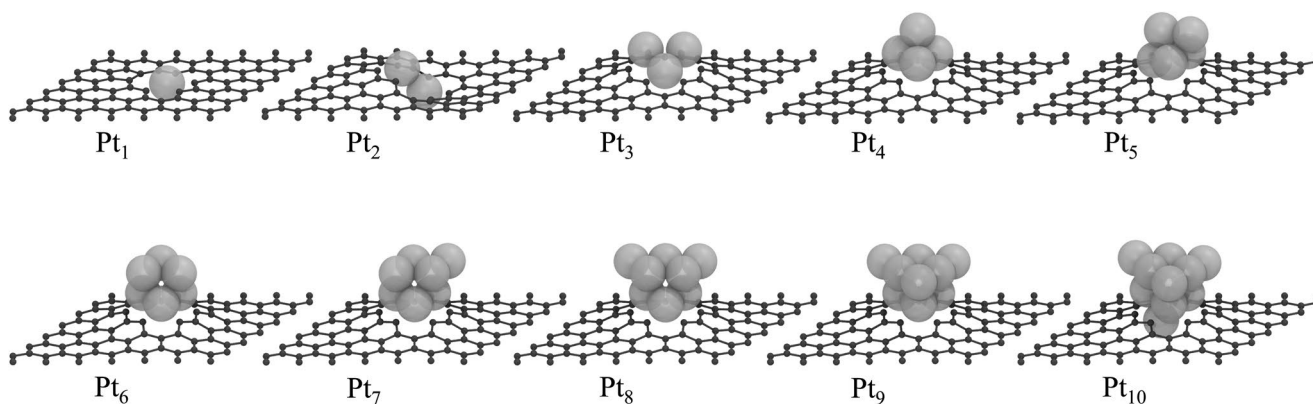


Figure 2. Configurations of the growth of Pt_n clusters with $n \leq 10$ Pt atoms on a d_4 graphene sheet resulting from the removal of 4 C atoms.

Due to the strong Pt–C σ -bonds, as indicated by the adsorption energy values of a single Pt atom on the different defective graphene supports (5.1–8.3 eV; see Table S1, Supporting Information), initial cluster growth occurs always directly at the defect site.

For all Pt configurations, asymmetric Pt cluster growth on one side of the (defective) graphene layer is calculated to be most stable (see Figure S2, Supporting Information). **Figure 2** illustrates the evolution of the Pt cluster with up to ten Pt atoms on the highly symmetric d_4 graphene support as an example, forming an inverted pyramid with the tip anchored in the defect. All other defective graphene structures do not exhibit such symmetry but show a localized spin density associated with higher reactivity around the vacancy (see Figure S3, Supporting Information). As a result, the Pt clusters grown on less symmetric defects (compared to d_4) also exhibit less symmetric structures in their lowest-energy configurations. This

result seems to emphasize the templating effect of the defects, not only with regards to the size of the cluster that is easily accommodated but also with regards to which shape that clusters grows into. The structures of all Pt_{10} clusters on the defective supports are illustrated in **Figure 3**.

For Ni, it was found that clusters prefer to grow symmetrically on both sides of the defective graphene sheet;^[23] such configurations are found to be less stable than asymmetrically grown clusters in the case of Pt. These different cluster arrangements are most likely the result of differences between the cohesive energy of fcc-Pt and fcc-Ni. In the case of nickel, the cohesive energy is calculated to be 4.61 eV atom⁻¹ (exp: 4.44 eV atom⁻¹),^[35] while platinum has a calculated cohesive energy of 5.49 eV atom⁻¹ (exp: 5.85 eV atom⁻¹).^[35] The formation of Pt–Pt bonds is therefore energetically more favorable than formation of Ni–Ni bonds which results in a preference for asymmetric cluster growth in the case of Pt.

For defect sizes corresponding to three or more missing C atoms, a single Pt atom is directly embedded in the graphene layer (see Figure S2, Supporting Information). In the case of smaller defects, Pt atoms prefer to accumulate on top of the graphene layer. This change in binding geometry affects the stability of the resulting graphene-cluster system. To illustrate this trend, Figure 1 shows the binding energy per Pt atom as a function of the adsorbed Pt cluster size for graphene supports with 0 to 5 defects.

Several noteworthy trends emerge from this analysis. First, the binding energy per atom becomes more exothermic as the number of defects increases. This trend is mostly independent of the Pt cluster size except for the smallest cluster sizes ($n = 1, 2$) where the cluster stability is reduced for the largest defects (d_4 and d_5). This can be attributed to a size mismatch between the smallest clusters and the largest defects. Furthermore, the deviation is stronger in the case of d_4 than for d_5 . An explanation for the exceptional behavior of the d_4 defect can be found in the electronic structure of the d_4 system: spin density analysis of this system (see Figure S3, Supporting Information) indicates that unlike for any other system, the d_4 defect is fully delocalized over the entire model system, thereby stabilizing the defect significantly. By comparison, the spin density distribution of the other defect systems is rather localized around the vacancy.

Second, focusing on clusters with $n > 2$, the binding energy increases in distinct steps as a function of the number of

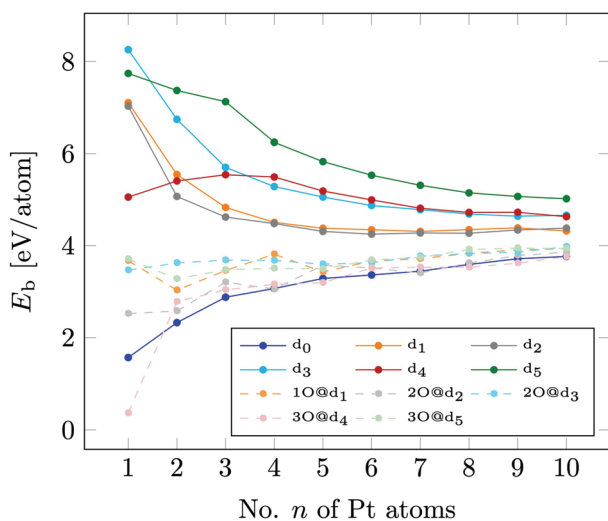


Figure 1. Binding energy E_b in eV per Pt atom for the growth of Pt_n clusters on graphene supports with various vacancy defects d_n , resulting from the removal of $x \leq 5$ C atoms (solid lines). For comparison, the dashed lines show the binding energy values of the energy-minimized atomic configurations resulting from Pt clusters formed during systematic growth on the unoxidized graphene supports transferred onto the oxidized defective graphene models.

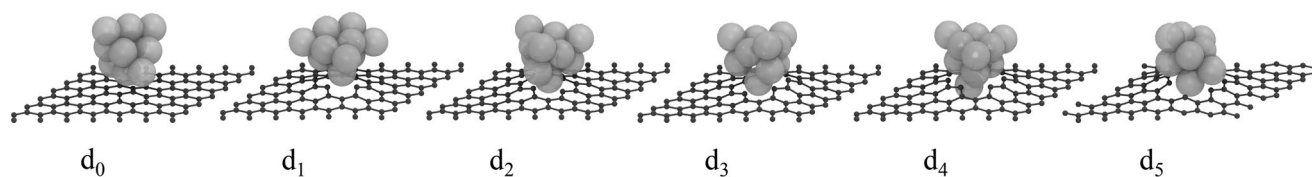


Figure 3. Configurations of Pt₁₀ clusters on graphene sheets with various defect sizes (d₀–d₅).

defects. The binding energy on d₁ and d₂ is significantly larger than on d₀ due to the initial presence of unsaturated C bonds which interact more strongly with Pt atoms compared to d₀ where interactions take place between *d*-orbitals of the Pt atoms and the π -system of graphene. Another distinct jump in E_b is observed for d₃ and d₄ which are large enough to accommodate a Pt atom within the graphene plane, thereby introducing more Pt–C bonds. Finally, the last jump is observed for d₅ where more than one Pt atom can potentially be located within the graphene plane.

Third, for the defect systems d₁ to d₅, E_b : i) continuously reduces with increasing Pt cluster size and ii) is converged upon reaching a cluster size of Pt₁₀. For the defect-free d₀ system, a continuous increase of E_b is observed with increasing cluster size and convergence is not yet observed upon reaching Pt₁₀. These trends therefore seem to suggest a templating effect of the graphene defects which limits the size of clusters that are most favorable to form on these systems. On the other hand, Pt clusters on defect-free graphene are thermodynamically favored to grow to larger sizes. This difference in behavior is most likely a result of the competition between formation of Pt–C and Pt–Pt bonds on defective systems whereas growth is almost exclusively driven by formation of Pt–Pt bonds on the defect-free support.

2.2. Electronic Structure Analysis of the Graphene–Pt-Cluster Combined Material

The strong binding between the non-oxidized platinum clusters and the defective carbon sheets is further analyzed with respect to the electronic structure of the combined material. At the graphene–metal interface, charge-density-difference analysis shows a significant redistribution of charge, suggesting bond formation between the Pt cluster and the support (see Figure S4, Supporting Information). Consistent with the spin density analysis and in accordance with previously literature,^[30,36] Bader charge analysis quantitatively shows that Pt atoms further away from the graphene layer are electron-rich - that is, carrying negative partial charge - while those at the Pt cluster/graphene interface show positive values, indicating charge transfer to the graphene support (see Figure S4, Supporting Information).

Figure S5, Supporting Information, shows the sum of Bader charges on all Pt atoms as a function of the Pt cluster size on d₀ to d₅ vacancy defect systems. The sum of Bader charges oscillates with increasing Pt cluster size on the same support. For defect-free graphene, the sum of Bader charges is zero on average, indicating that no significant charge transfer takes place. For d₁ to d₅, on average the sum of Bader charges on the

Pt cluster increases with the size of the defect. A point of saturation is reached for the d₂ defect at which point $\approx 0.4 e$ are transferred to the support in total. This number remains approximately the same for larger defects and does not strongly depend on the size of the Pt cluster. This analysis indicates that charge transfer to the graphene support is mainly governed by the electronic structure of the (defective) graphene support and less by the size of the Pt cluster. Therefore, if the goal is to tune the electronic structure of a graphene–Pt-cluster combined material toward being more nucleophilic or electrophilic, changing the vacancy defect structure of the graphene support will result in more significant changes in reactivity compared to changing the cluster size in the size range computed in this study.

2.3. Stability of Pt Clusters on Oxidized Graphene Supports

Studies on the adsorption of a Pt₁₃ cluster on pristine graphene and graphene oxide with a specific oxygen to carbon ratio show, according to literature, that specific O/C proportions can lead to an increase in cluster adsorption strength.^[29] In this section, the influence of the presence of oxygen in defective graphene substrates d_x ($x \leq 5$) for Pt_n clusters of different sizes ($n \leq 10$) is investigated. The binding energy of Pt clusters is studied as a function of the degree of oxidation of the defects (dashed lines in Figure 1). The number of oxygen atoms was chosen so that all carbon five-membered rings around the vacancies were saturated (see Figure S6, Supporting Information). All platinum clusters formed during systematic growth on the oxygen-free graphene supports were placed on the oxidized defective graphene models and the resulting atomic configurations were energy-minimized.

The dashed lines in Figure 1 illustrate that fully oxidizing the defects results in a homogenization of the binding energy values, with all systems showing E_b trends following that of the d₀ system rather than that of the non-oxidized parent systems. Since oxygen saturates all C-sp² orbitals, strong Pt–C bonds cannot be formed and the binding energy values of the Pt clusters on all oxidized defects is approximately equal to the binding energy of the Pt clusters on defect-free non-oxidized graphene.

In order to quantify the impact of oxidation on the binding energy of Pt clusters further, E_b was calculated as a function of increasing number of oxygen atoms located in the various defects (see Figures S7 and S8, Supporting Information). In general, the trend shows that the cluster binding energy systematically reduces as the degree of oxidation of the tested vacancy defect models increases, with oxygen-free surfaces showing the strongest binding. These trends suggest that saturation of dangling C bonds with oxygen leaves those bonds unable to form Pt–C bonds. The formation of Pt–C bonds is

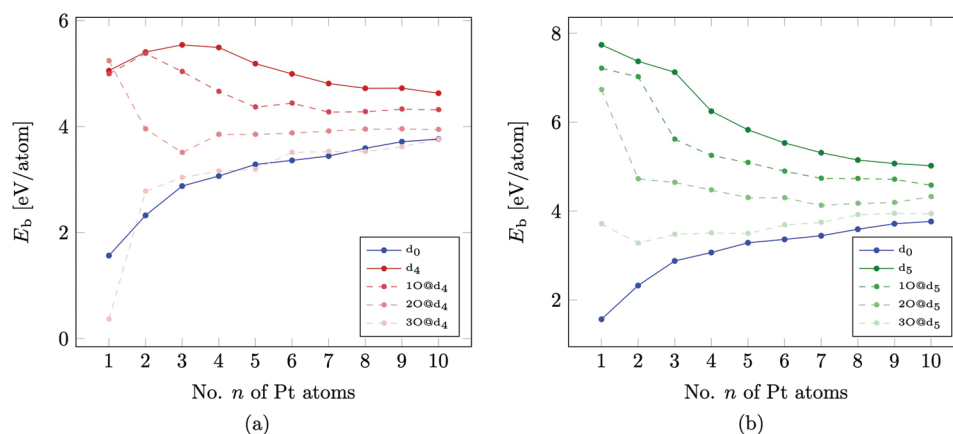


Figure 4. Comparison of the binding energy E_b in eV per Pt atom for the geometry optimized Pt_n configurations on gradually oxidized a) d_4 graphene supports (red dashed lines) and b) d_5 graphene supports (green dashed lines) with the growth of Pt_n clusters on d_0 and d_4 or d_5 graphene sheets (solid lines).

therefore shown to stabilize Pt clusters support material interactions more strongly than formation of C–O–Pt bonds.

Figure 4a illustrates the effect of increasing oxidation exemplarily for the d_4 graphene system while **Figure 4b** confirms this trend for d_5 systems. In both cases, the binding energy of clusters with more than two Pt atoms is most similar to the trend obtained for defect-free graphene (d_0). On a defective d_5 graphene surface with a single oxygen atom, the Pt clusters are less strongly bound to the support by up to 0.8 eV per Pt atom. The doubly-oxidized graphene supports show a 0.26 eV per Pt atom weaker bonding between the Pt clusters and the surface at cluster sizes above $n = 7$ compared to the singly-oxidized support.

The results shown in **Figures 1** and **4** were obtained by placing the converged Pt cluster configurations obtained on oxygen-free systems onto the oxidized models and subsequent energy minimization. To investigate if clusters will form differently on a previously oxidized support, Pt atoms were also added consecutively to the d_4 model and energy-minimized after each addition. **Figure S9**, Supporting Information, compares the results of the stepwise approach with the results of the ad hoc addition and subsequent energy-minimization of pre-formed clusters shown in **Figure 4a**.

Even though the optimized cluster configurations were indeed found to be different for the stepwise and the ad hoc addition approach, the resulting E_b ultimately did not vary significantly. The deviation is below 0.17 eV per Pt atom for systems with $n \geq 4$ Pt atoms. This result indicates that cluster stability is predominantly determined by the number of Pt–Pt, Pt–C, and Pt–O bonds rather than the exact cluster geometry. We expect that this trend is only valid for small clusters. As soon as NPs become large enough to express defined surface facets, the stability of the particle will strongly depend on the type of facet and, therefore, on the NP structure.

2.4. Competition between Oxidation of Cluster and Support

Based on the result that Pt cluster adhesion is significantly reduced on an oxidized defective graphene support, the

question arises whether a graphene–Pt-cluster combined material previously synthesized under oxygen-free conditions remains stable when brought into contact with oxygen afterward, for example when used as an ORR catalyst. To examine this question, the relative stability of oxygen atoms adsorbed at different sites on the model system is compared.

We find that for the present model systems, spin density analysis can be used to predict the most reactive sites on the model systems for those cases where calculations converged to a solution with a net spin surplus. In the case of the non-oxidized graphene-cluster combined model systems, we consistently find surplus spin density localized on the Pt atoms farthest away from the graphene surface. Screening of adsorption sites with oxygen atoms confirms that these sites, indeed, give rise to the most exothermic adsorption energy.

Figure 5 illustrates this circumstance for a $Pt_{10}@d_4$ system (**Figure 5a**), where the spin density analysis (**Figure 5b**) indicates that the topmost Pt atoms should be most reactive. **Figure 5c** shows the most stable oxygen adsorption position which is in agreement with the spin density prediction. In general, calculations show that corner atoms of inverted pyramid cluster configurations are most favorable for oxygen adsorption (see **Figures S10** and **S11**, Supporting Information).

Figure 6a shows the adsorption energy of a single oxygen atom on the Pt_{10} cluster and in the graphene vacancy defect d_x as a function of the size of the vacancy ($x = 0–5$). Graphene supports with $x = 3$ or 4 missing C atoms represent special cases where the oxygen atom adsorbs with approximately the same strength regardless whether the oxygen binds to the platinum cluster or in the defect. The reason for this behavior is likely the result of the interplay of specific cluster geometry and defect size. Depending on the geometry and anchoring of the platinum clusters in the oxidized defect, stabilizing Pt–O bonds can form under specific conditions. These bonds are formed in the Pt_{10} systems based on the single oxidized d_3 and d_4 graphene supports, thereby stabilizing the system (see **Figure S12**, Supporting Information). On the other hand, the oxygen atom is isolated and does not interact with the platinum cluster on the supports with $x = 1, 2,$ and 5 missing C atoms, which leads to less favorable oxygen adsorption energetics. This result is in

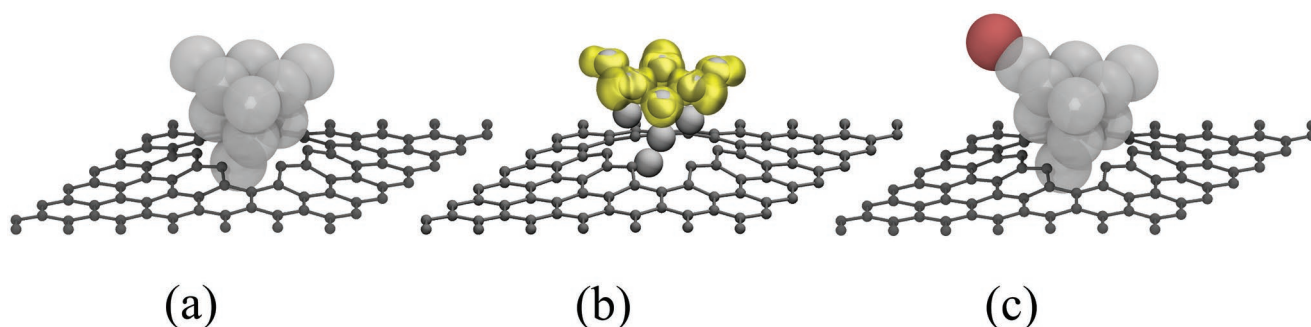


Figure 5. Prediction of the oxygen adsorption position on a) a $\text{Pt}_{10}@d_4$ cluster b) using the spin density analysis for an indication of the most reactive site in the cluster where c) the oxygen atom (red) binds energetically most stable.

agreement with literature reports detailing that specific O/C ratios give rise to increased binding strength of a Pt_{13} cluster.^[29]

In Section 2.3, results were established that suggested that Pt clusters are bound more weakly if the defective graphene support has been oxidized before clusters are introduced. The results presented in this section now suggest that the oxidation of the platinum cluster is usually more favorable than the oxidation of the vacancy defect.

Figure 6b shows the oxygen adsorption energy on the Pt cluster and in the defect as a function of the cluster size and a constant vacancy defect size d_2 (gray) and d_4 (red). For the d_2 support, adsorption of an oxygen atom on the Pt cluster appears to be more stable for $n \geq 2$ Pt atoms. The same trend can be found for d_4 graphene, with a few exceptions in this particular case. For Pt_3 and Pt_4 as well as Pt_{10} and Pt_{11} clusters on d_4 graphene, oxidation of the Pt cluster and oxidation of the defect are similarly favorable. We assume that this behavior is related to the delocalized charge density illustrated in Figure S3, Supporting Information. However, in order to be able to describe exactly why the oxygen adsorption at certain cluster sizes is energetically degenerate, regardless of whether the oxygen atom adsorbs on the cluster or in the defect, further simulations have to be performed.

In summary, Figure 6b illustrates that in most cases the presence of oxygen does not lower the binding energy of the

platinum cluster on graphene since the adsorption of oxygen on the cluster is preferred. The notable exception to this trend is the d_4 defect where for specific cluster sizes, oxygen adsorption on the cluster and in the defect is similarly favorable.

3. Conclusion

In summary, investigations of Pt_n cluster growth with $n \leq 10$ platinum atoms on perfect and defective graphene sheets reveal asymmetric cluster growth on only one side of the support, in contrast to literature reports for Ni cluster growth on defective graphene.^[23] The binding energy values of Pt_n clusters on various support materials d_x with $x \leq 5$ removed C atoms were obtained using DFT calculations. Larger defects in the graphene supports result in stronger bonding between the platinum cluster and the support. For the same vacancy size and increasing Pt cluster size, we calculate that the binding energy reduces systematically. On the other hand, the binding energy of clusters of increasing size on defect-free graphene systematically increases. We therefore conclude that vacancy defects seem to have a templating effect that can limit the size of Pt clusters growing on them while pristine graphene promotes continuous growth. Bader charge analysis shows that charge accumulation on the cluster mainly depends on the size of

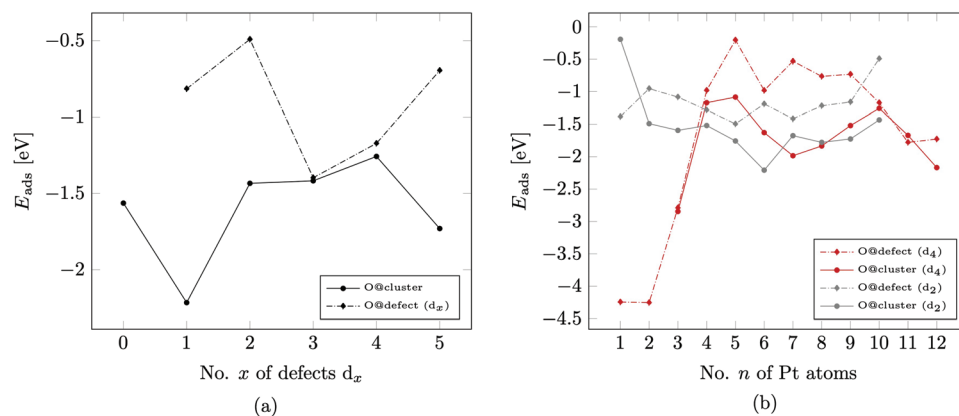


Figure 6. Adsorption energy E_{ads} (eV) of oxygen atoms a) on the Pt_{10} clusters on graphene supports with various vacancy defects (d_0 – d_5) (solid black line) and b) on Pt_n clusters with $n \leq 12$ Pt atoms on a d_2 (solid gray line) and a d_4 (solid red line) graphene support. For comparison, the dashed lines show the oxygen adsorption energy on the corresponding defective support at the interface between the d_x graphene support and the Pt cluster.

defects of the support and less on the number of Pt atoms in the cluster. Hence, to change the reactivity of the combined material, changing the support should be given higher priority than changing the cluster size.

Stepwise oxidation of the vacancy defects leads to systematic reduction of the binding energy of Pt clusters. Cluster binding energy results calculated for fully oxidized defects are similar to those obtained for defect-free non-oxidized graphene, indicating that Pt–C bonds contribute more strongly to the stabilization of Pt clusters on the support than the Pt–O–C bonds which form when vacancies are oxidized.

This result has significant implications guiding experimental efforts to synthesize such combined materials: because E_b of the Pt clusters is significantly reduced on oxidized defects, and because the E_b trend is reversed for the fully oxidized defects compared to the non-oxidized parent systems (that is, increase of E_b with cluster size rather than reduction), we suggest that oxygen-free synthesis conditions and graphene educts are key to generate materials where small-sized Pt clusters are strongly bound to the vacancy graphene substrate. This suggestion also implies that wet-chemical synthesis methods such as Hummer's method, where graphite is fully oxidized to exfoliate graphene oxide sheets before subsequent reduction to graphene,^[33] should be avoided to reduce the risk of oxidized vacancy defects in the material.

Furthermore, we find that oxygen adsorption on top of the platinum cluster is usually more stable compared to adsorption on the defect. This trend is not dependent of the size of the defect or the platinum cluster and can be predicted using spin density analysis. We therefore conclude that once the combined material has been successfully synthesized in an oxygen-free environment, oxidative degradation should be impeded because oxidation of the cluster is more favorable. This result indicates that such Pt/C combined materials are interesting ORR catalyst candidates. The notable exception to this trend is the d_4 support for which oxidation of Pt clusters and oxidation of the support are in competition in the case of specific cluster sizes. We attribute this exceptional behavior to the unique electronic structure of this defect which results from its high symmetry compared to the other tested defect systems.

Finally, we note that the formation energy of Pt clusters on defective graphene substrates in the size range studied in this work mostly depends on the number and ratio between Pt–C, Pt–Pt, and Pt–O bonds; the specific cluster geometry is secondary.

While in the present work the aim was to investigate the interaction between platinum catalyst and the underlying support, where solvation effects are expected to be less relevant, this is certainly not the case for any catalytic process occurring on the catalyst surface itself. In our previous studies on the ORR on platinum^[37,38] we could clearly quantify the strong impact of solvation. Thus, in our future works that will concentrate on the reaction mechanisms on the supported platinum catalysts the impact of the water surrounding will certainly be taken into account.

4. Computational Section

All periodic DFT calculations were performed using the Vienna ab initio Simulation Package (VASP), version 6.2.0.^[39–42] To rep-

resent valence electrons, the smooth parts of the wave functions are expanded according to the VASP code in a plane wave basis set with an energy limit of 600 eV; see Figure S13, Supporting Information, for detailed convergence test results. To describe the influence of inner electrons, the projector-augmented wave method (PAW)^[43,44] was used. The spin-polarized exchange correlation functional by Perdew, Burke, and Enzerhof (PBE) within the generalized gradient approximation (GGA) was used for the simulations.^[45,46] To rule out interactions beyond the periodic boundary conditions, convergence tests and a spin density analysis (see Figures S14 and S3, Supporting Information) of the graphene model confirmed the sufficiency of 7×7 supercells with 98 atoms assuming a non-defective graphene sheet. The length of the graphene C–C bond at equilibrium is determined to be 1.425 Å from which model systems are constructed. A vacuum region of ≈ 29 Å separates the periodic images in the vertical z -direction. For these large systems, evaluation in real space is used for the projection operators. All calculations are performed using a converged $3 \times 3 \times 1$ Γ -centered k -point mesh; see Figure S15, Supporting Information, for detailed convergence test results. To accelerate convergence of the self-consistent optimization of the wave function, a Gaussian smearing with a smearing width of 0.01 eV is used. Once the difference in total energy is below $e-5$ eV, the electronic self-consistent field is considered converged. The atomic coordinates are relaxed until the norms of all forces fall below 5×10^{-3} eV Å⁻¹. The limited-memory Broyden–Fletcher–Goldfarb–Shanno (LBFGS) algorithm, as implemented in the transition state tools for VASP (VTST) by the Henkelman group, is used for structural relaxation.

For a Pt cluster adsorbed on graphene, the binding energy E_b is referenced to the energy of the corresponding graphene support E_{graphene} and the number n of isolated Pt atoms with total energy $E_{\text{Pt,isolated}}$ in the particular cluster:

$$E_b = -(E_{\text{Pt}_n/\text{graphene}} - E_{\text{graphene}} - n \cdot E_{\text{Pt,isolated}}) / n \quad (1)$$

where $E_{\text{Pt}_n/\text{graphene}}$ represents the total energy of the bound $\text{Pt}_n/\text{graphene}$ system. Analogous calculations are performed for the binding energy of Pt_n clusters on oxidized graphene substrates, where $E_{\text{Pt}_n/\text{graphene}}$ is replaced by $E_{\text{Pt}_n/\text{graphene/O}}$ and E_{graphene} is replaced by $E_{\text{graphene/O}}$.

Finally, the oxygen adsorption energy E_{ads} is defined as

$$E_{\text{ads}} = E_{\text{Pt}_n/\text{graphene/O}} - E_{\text{Pt}_n/\text{graphene}} - \frac{1}{2} E_{\text{O}_2} \quad (2)$$

where E_{O_2} is the total energy of an isolated oxygen molecule.

Supporting Information

Supporting Information is available from the Wiley Online Library or from the author.

Acknowledgements

The authors acknowledge support by the German Research Foundation (DFG) through the Sonderforschungsbereich (collaborative research centers) SFB-1316 (project-ID: 327886311). Further, the authors acknowledge the computer time supported by the state of Baden-Württemberg

through the bwHPC project and the DFG through grant number INST40/467-1 FUGG.

Open access funding enabled and organized by Projekt DEAL.

Conflict of Interest

The authors declare no conflict of interest.

Data Availability Statement

The data that support the findings of this study are available from the corresponding author upon reasonable request.

Keywords

atomistic modeling, degradation, density functional theory, fuel cells, graphene vacancy defects, oxidation, platinum clusters

Received: November 30, 2022

Revised: December 20, 2022

Published online:

- [1] S. Sui, X. Wang, X. Zhou, Y. Su, S. Riffat, C.-j. Liu, *J. Mater. Chem. A* **2017**, *5*, 1808.
- [2] X. Yu, S. Ye, *J. Power Sources* **2007**, *172*, 133.
- [3] K. Yamamoto, T. Imaoka, W.-J. Chun, O. Enoki, H. Katoh, M. Takenaga, A. Sonoi, *Nat. Chem.* **2009**, *1*, 397.
- [4] I. Fampiou, A. Ramasubramaniam, *J. Phys. Chem. C* **2012**, *116*, 6543.
- [5] H. Shi, S. M. Auerbach, A. Ramasubramaniam, *J. Phys. Chem. C* **2016**, *120*, 11899.
- [6] G. Centi, M. Gangeri, M. Fiorello, S. Perathoner, J. Amadou, D. Bégin, M. Ledoux, C. Pham-Huu, M. Schuster, D. Su, J.-P. Tessonnier, R. Schlögl, *Catal. Today* **2009**, *147*, 287.
- [7] Y. Li, Y. Li, E. Zhu, T. McLouth, C.-Y. Chiu, X. Huang, Y. Huang, *J. Am. Chem. Soc.* **2012**, *134*, 12326.
- [8] E. Lam, J. H. Luong, *ACS Catal.* **2014**, *4*, 3393.
- [9] I. C. Gerber, P. Serp, *Chem. Rev.* **2020**, *120*, 1250.
- [10] X. Duan, J. Xu, Z. Wei, J. Ma, S. Guo, S. Wang, H. Liu, S. Dou, *Adv. Mater.* **2017**, *29*, 1701784.
- [11] J. C. Meier, C. Galeano, I. Katsounaros, J. Witte, H. J. Bongard, A. A. Topalov, C. Baldizzone, S. Mezzavilla, F. Schüth, K. J. J. Mayrhofer, *Beilstein J. Nanotechnol.* **2014**, *5*, 44.
- [12] X. Yu, S. Ye, *J. Power Sources* **2007**, *172*, 145.
- [13] S. Zhang, X.-Z. Yuan, J. N. C. Hin, H. Wang, K. A. Friedrich, M. Schulze, *J. Power Sources* **2009**, *194*, 588.
- [14] P. J. Ferreira, G. J. la O', Y. Shao-Horn, D. Morgan, R. Makharia, S. Kocha, H. A. Gasteiger, *J. Electrochem. Soc.* **2005**, *152*, A2256.
- [15] Y. Shao-Horn, P. Ferreira, G. la O', D. Morgan, H. A. Gasteiger, R. Makharia, *ECS Trans.* **2006**, *1*, 185.
- [16] K. Schlögl, K. J. Mayrhofer, M. Hanzlik, M. Arenz, *J. Electroanal. Chem.* **2011**, *662*, 355.
- [17] W. Wang, S. Yao, S. Deng, Y. Wang, C. Qiu, C. Mao, J.-g. Wang, *Langmuir* **2021**, *37*, 12529.
- [18] D.-H. Lim, J. Wilcox, *J. Phys. Chem. C* **2011**, *115*, 22742.
- [19] I. Fampiou, A. Ramasubramaniam, *J. Phys. Chem. C* **2013**, *117*, 19927.
- [20] Y. Okamoto, *Chem. Phys. Lett.* **2006**, *420*, 382.
- [21] H. Wang, Q. Wang, Y. Cheng, K. Li, Y. Yao, Q. Zhang, C. Dong, P. Wang, U. Schwingenschlögl, W. Yang, X. X. Zhang, *Nano Lett.* **2012**, *12*, 141.
- [22] F. Banhart, J. Kotakoski, A. V. Krasheninnikov, *ACS Nano* **2011**, *5*, 26.
- [23] W. Gao, J. Mueller, J. Anton, Q. Jiang, T. Jacob, *Angew. Chem., Int. Ed. Engl.* **2013**, *52*, 14237.
- [24] S. Sahoo, M. E. Gruner, S. N. Khanna, P. Entel, *J. Chem. Phys.* **2014**, *141*, 074707.
- [25] Y. Li, Z. Zhou, G. Yu, W. Chen, Z. Chen, *J. Phys. Chem. C* **2010**, *114*, 6250.
- [26] M. Zhou, A. Zhang, Z. Dai, C. Zhang, Y. P. Feng, *J. Chem. Phys.* **2010**, *132*, 194704.
- [27] S. K. Kaiser, Z. Chen, D. F. Akl, S. Mitchell, J. Pérezpérez-Ramírez, *Chem. Rev.* **2020**, *120*, 11703.
- [28] H.-Y. Zhuo, X. Zhang, J.-X. Liang, Q. Yu, H. Xiao, J. Li, *Chem. Rev.* **2020**, *120*, 12315.
- [29] S.-Y. Wu, J.-J. Ho, *J. Phys. Chem. C* **2014**, *118*, 26764.
- [30] G. Ramos-Sanchez, P. Balbuena, *Phys. Chem. Chem. Phys.* **2013**, *15*, 11950.
- [31] G. Yang, X. Fan, S. Shi, H. Huang, W. Zheng, *Appl. Surf. Sci.* **2017**, *392*, 936.
- [32] J.-g. Wang, Y.-a. Lv, X.-n. Li, M. Dong, *J. Phys. Chem. C* **2009**, *113*, 890.
- [33] W. S. J. Hummers, R. E. Offeman, *J. Am. Chem. Soc.* **1958**, *80*, 1339.
- [34] J. Ma, A. Habrioux, Y. Luo, G. Ramos-Sanchez, L. Calvillo, G. Granozzi, P. B. Balbuena, N. Alonso-Vante, *J. Mater. Chem. A* **2015**, *3*, 11891.
- [35] P. Janthon, S. A. Luo, S. M. Kozlov, F. Viñes, J. Limtrakul, D. G. Truhlar, F. Illas, *J. Chem. Theory Comput.* **2014**, *10*, 3832.
- [36] I. Fampiou, A. Ramasubramaniam, *J. Phys. Chem. C* **2012**, *116*, 6543.
- [37] T. Jacob, *Fuel Cells* **2006**, *6*, 159.
- [38] S. Venkatchalam, T. Jacob, *Density Functional Theory Applied to Electrocatalysis*, John Wiley & Sons, Ltd, Hoboken, NJ **2010**.
- [39] G. Kresse, J. Hafner, *Phys. Rev. B* **1993**, *47*, 558.
- [40] G. Kresse, J. Furthmüller, *Phys. Rev. B* **1996**, *54*, 11169.
- [41] G. Kresse, J. Furthmüller, *Comput. Mater. Sci.* **1996**, *6*, 15.
- [42] G. Kresse, J. Hafner, *Phys. Rev. B* **1994**, *49*, 14251.
- [43] P. E. Blöchl, *Phys. Rev. B* **1994**, *50*, 17953.
- [44] G. Kresse, D. Joubert, *Phys. Rev. B* **1999**, *59*, 1758.
- [45] J. P. Perdew, K. Burke, M. Ernzerhof, *Phys. Rev. Lett.* **1996**, *77*, 3865.
- [46] Y. Zhang, W. Yang, *Phys. Rev. Lett.* **1998**, *80*, 890.